Pyrene Functionalized Norbornadiene-Quadricyclane Fluorescent Photoswitches: Characterization of their Spectral Properties and

Chemistry–A European Journal

Research Article
doi.org/10.1002/chem.202400322

Chemistry Europe
European Chemical Societies Publishing

www.chemeurj.org

Pyrene Functionalized Norbornadiene-Quadricyclane Fluorescent Photoswitches: Characterization of their Spectral Properties and Application in Imaging of Amyloid Beta Plaques

Shima Ghasemi,[a] Monika Shamsabadi,[a] Axel Olesund,[a] Francisco Najera,[b, c] Andreas Erbs Hillers-Bendtsen,[d] Fredrik Edhborg,[a] Adil S. Aslam,[a] Wera Larsson,[a] Zhihang Wang,[e] Francoise M. Amombo Noa,[a] Rebecca Jane Salthouse,[j] Lars Öhrström,[a] Helen Hölzel,[j] E. Perez-Inestrosa,[b, c] Kurt V. Mikkelsen,[d] Jörg Hanrieder,[f, g] Bo Albinsson,[a] Ambra Dreos,*[b, f] and Kasper Moth-Poulsen*[a, h, i, j]

This study presents the synthesis and characterization of two fluorescent norbornadiene (NBD) photoswitches, each incorporating two conjugated pyrene units. Expanding on the limited repertoire of reported photoswitchable fluorescent NBDs, we explore their properties with a focus on applications in bioimaging of amyloid beta (Aβ) plaques. While the fluorescence emission of the NBD decreases upon photoisomerization, aligning with what has been previously reported, for the first time we observed luminescence after irradiation of the quadricyclane (QC) isomer. We deduce how the observed emission is induced by photoisomerization to the excited state of the parent isomer (NBD) which is then the emitting species. Thorough characterizations including NMR, UV-Vis, fluorescence, X-ray structural analysis and density functional theory (DFT) calculations provide a comprehensive understanding of these systems. Notably, one NBD-QC system exhibits exceptional durability. Additionally, these molecules serve as effective fluorescent stains targeting Aβ plaques in situ, with observed NBD/QC switching within the plaques. Molecular docking simulations explore NBD interactions with amyloid, unveiling novel binding modes. These insights mark a crucial advancement in the comprehension and design of future photochromic NBDs for bioimaging applications and beyond, emphasizing their potential in studying and addressing protein aggregates.

[a] S. Ghasemi, M. Shamsabadi, A. Olesund, F. Edhborg, A. S. Aslam, W. Larsson, F. M. Amombo Noa, L. Öhrström, B. Albinsson, K. Moth-Poulsen
Department of Chemistry and Chemical Engineering,
Chalmers University of Technology,
41296 Gothenburg, Sweden
E-mail: kasper.moth-poulsen@upc.edu

[b] F. Najera, E. Perez-Inestrosa, A. Dreos
Instituto de Investigación Biomédica de Málaga y Plataforma en Nanomedicina-IBIMA Plataforma Bionand,
29590 Malaga, Spain
E-mail: ambra.dreos@gu.se

[c] F. Najera, E. Perez-Inestrosa
Departamento de Química Orgánica, Facultad de Ciencias,
Universidad de Málaga,
29071 Málaga, Spain

[d] A. Erbs Hillers-Bendtsen, K. V. Mikkelsen
Department of Chemistry,
University of Copenhagen,
Universitetsparken 5, Copenhagen Ø, Denmark

[e] Z. Wang
Department of Materials Science and Metallurgy,
University of Cambridge,
27 Charles Babbage Rd, Cambridge CB3 0FS, U.K.

[f] J. Hanrieder, A. Dreos
Department of Psychiatry and Neurochemistry,
Sahlgrenska Academy,
University of Gothenburg,
43180 Mölndal, Sweden

[g] J. Hanrieder
Department of Neurodegenerative Disease,
Queen Square Institute of Neurology,
University College London,
London WC1N 3BG, UK.

[h] K. Moth-Poulsen
The Institute of Materials Science of Barcelona,
ICMAB-CSIC,
Bellaterra, 08193 Barcelona, Spain

[i] K. Moth-Poulsen
Catalan Institution for Research & Advanced Studies,
ICREA,
Pg. Llu'ıs Companys 23, 08010 Barcelona, Spain

[j] R. J. Salthouse, H. Hölzel, K. Moth-Poulsen
Department of Chemical Engineering,
Universitat Politècnica de Catalunya,
EEBE, Eduard Maristany 10–14, 08019 Barcelona, Spain

Supporting information for this article is available on the WWW under https://doi.org/10.1002/chem.202400322

Introduction

Molecular photoswitches are a class of molecules that undergo reversible structural and property changes upon irradiation with an appropriate light source. Fluorescent photoswitches constitute a subclass of molecular switches that exhibit photochromism; they are fluorescent in one or two of the isomer forms, therefore their emission is toggled ON/OFF or otherwise manipulated by means of photoirradiation. Photochromic molecules have been widely used for different applications such as photochromic glasses,[1] fluorescent labelling and bioimaging,[2] super-resolution microscopy,[3] photopharmacology,[4] and others. Several examples of different classes of fluorescent photoswitches include diarylethenes, anthracenes, stilbenes, azo-based compounds, norbornadienes, and spiropyrans.[5]

Photoswitchable fluorescent dyes for bioimaging applications have several advantages,[6] as for example advanced probing properties, multi-stimuli responsive and functional biosensors,[7] improved signal quality,[8] decreased photobleaching[9] and access to a series of advanced imaging techniques such as super resolution imaging.[2c,10] The norbornadiene-quadricyclane (NBD-QC) photoswitch system has been investigated for different applications such as solar energy storage,[11] molecular electronics,[12] and bioimaging.[13] Norbornadiene (NBD) derivatives isomerize to highly strained quadricyclane (QC) by photoirradiation and convert back to NBD either by thermal,[14] catalytic[11a] or light-induced activation.[15] Only a few photoswitchable fluorescent NBDs have been reported, and the in-depth understanding of their properties is of relevance for a range of applications, including bioimaging of protein aggregates. Previously, Dreos *et al.* investigated a photoswitchable fluorescent norbornadiene (a bis(ethynylphenylene) substituted NBD) as an imaging probe for amyloid beta (Aβ) plaques in Alzheimer disease (AD) mouse models.[13] Aβ protein aggregation is a major pathological hallmark of AD[16] and it recently emerged how Aβ aggregates are highly heterogeneous in their biochemical and morphological composition.[17] Unfortunately, the mechanism of Aβ aggregation and how Aβ toxicity is mediated is at present not fully understood. Gaining insights into how Aβ exerts its neurotoxic effects through changes in aggregation state and biochemical composition represents a fundamental goal in AD research. Aβ aggregation can be interrogated using fluorescent probes that exhibit aggregation-induced fluorescence,[18] and photoswitchable probes that change their spectral properties upon irradiation with light have further expanded the imaging field enabling advanced imaging techniques as discussed above.[2c] The previously investigated bis(ethynylphenylene) substituted NBD is able to target and recognize Aβ aggregates, delineating their heterogeneity thanks to hyperspectral properties upon binding; moreover, it was switched off and on in tissue. However, there are still several challenges to be addressed to utilize NBD derivatives for advanced bioimaging techniques.

Herein, we decided to further develop and explore NBD/QC systems for bioimaging applications. Pyrene derivatives have been extensively used to investigate biomolecules.[19] Their fluorescent properties are affected by the polarity of the microenvironment and by their intermolecular distance and orientation since they can form emissive excimers.[19] Moreover, pyrene-modified *trans*-stilbene salicylic acids have been successfully applied to target and study Aβ aggregation,[20] showing potential for applications as fluorescent probes of Aβ aggregates. Therefore, we decided to explore the combination of pyrene with the switchable norbornadiene unit to target Aβ aggregates and characterize and investigate the potential of such systems for bioimaging. For example, absorption and emission need to be red-shifted,[18] solubility in aqueous systems is needed for extended bio-applications,[18,21] and QC to NBD switching *in situ* needs to be orders of magnitude faster or fully light-controlled to access advanced imaging applications.[2c,3a,21]

The molecular structures of NBD-1Py and NBD-2Py and synthesis route is described in (Scheme 1). The molecular structures are functionalized with two pyrene groups linked via the 1 or 2 position of pyrene, symmetrically attached to the core NBD molecule. Surprisingly, the fluorescence and photoswitching properties of the two structural isomers are radically different, and show many interesting aspects, which required an extensive spectroscopic and computational investigation to be understood. Additionally, NBD-1Py and NBD-2Py are investigated for Aβ plaques imaging in AD mouse models.

Synthesis

The synthesis of NBD pyrene end-capped molecules is delineated in Scheme 1. 2,3-Dibromonorbornadiene was synthesized from norbornadiene according to the method described in the literature.[22] To synthesize NBD-1Py, 1-ethynylpyrene was reacted with di-bromo NBD *via* a Sonogashira reaction. The same procedure is applied for the synthesis of NBD-2Py using 2-ethynylpyrene as a starting material. The detailed

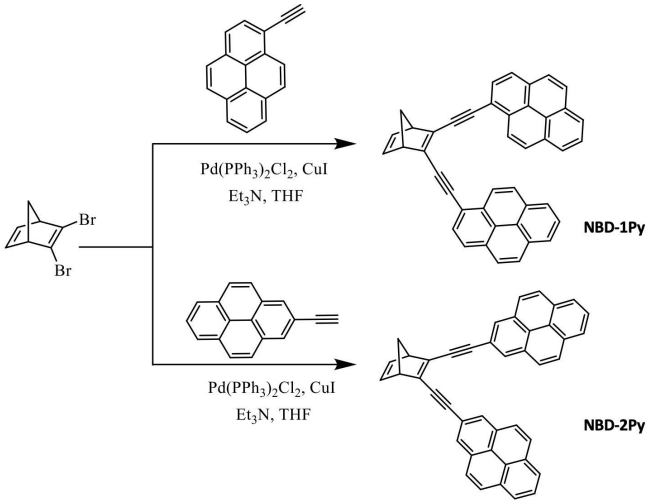

Scheme 1. Synthesis and molecular structures of NBD-1Py and NBD-2Py.

synthetic procedures and characterisation are reported in the Supporting Information (SI).

Spectroscopic Characterization

Both synthesized norbornadienes are fluorescent, and the absorption and emission spectra of NBD-1Py and NBD-2Py are shown in Figure 1a,b. Interestingly, the emission profiles are quite different in the two systems. Spectral characterizations are complemented with DFT calculations and natural transition orbitals for relevant transitions (See following discussion and SI Section 4 for more details). NBD-1Py has the highest fluorescence quantum yield (55% ±2%), while NBD-2Py has a fluorescence quantum yield of 19% ±2%. The emission lifetime of NBD-1Py is 2.1 ns, and for NBD-2Py it is 0.8 ns. From the fluorescence quantum yield and the fluorescence lifetime, the fluorescence rate constant was calculated. Note that it is almost identical for both NBD-1Py and NBD-2Py ($2.6\times10^8\ s^{-1}$ and $2.7\times10^8\ s^{-1}$ respectively), which indicates that competing processes such as non-radiative deactivation and photoisomerization are more prominent in NBD-2Py, aligning with the observed isomerization behaviours (*vide infra*). Upon irradiation using a 405 nm LED lamp, NBD-2Py photoswitches to the respective QC-isomer with near-quantitative conversion (Figure 1c). The parent isomer of QC-2Py was thermally recovered, and the half-life was calculated to be 15 minutes at room temperature. The quantum yield of the photoisomerization reaction ($\phi_{NBD\text{-}2Py\rightarrow QC\text{-}2Py}$) was measured to be 46%. On the other hand, when irradiating NBD-1Py it did not seem to photoisomerize to QC, but rather to degrade (see SI Figure S6 for NMR characterization). To rationalize the experimental observations, we calculated DFT optimized geometries and natural transition orbitals for relevant transitions. These calculations show good correlation with the experimental absorptions and emissions of the NBD-derivatives (see Table 1). The absorption and emission of NBD-1Py are bathochromically shifted (ca. 50 nm) with respect to the NBD-2Py. This can be explained by a better electronic interaction between the pyrene-ethynyl moiety and the NBD core in NBD-1Py. For this compound, the allowed transitions with a high value of their oscillator strength are the $S_1\leftarrow S_0$ and the $S_2\leftarrow S_0$ (see Table 1). For the first of these transitions the dominant component is LUMO←HOMO, for the second one the dominant components are LUMO←HOMO-1 and LUMO+1←HOMO. For NBD–1Py, the electronic density of the molecular orbitals involved in these transitions are distributed along the whole molecule. In contrast, for NBD-2Py only the transition $S_1\leftarrow S_0$ is allowed with a dominant component LUMO←HOMO (Table 1) for which only one of the pyrene rings are conjugated with the NBD core (see Figure 2). This behavior is in agreement with the photophysical properties of other previously describe ethynyl-pyrenes substituted in 1- or 2-positions.[23] This subtle difference likely provides also a qualitative explanation as to why NBD-2Py undergo photoisomerization to QC-2Py while NBD-1Py does not.

The photoswitching effect on the absorption and emission properties of NBD-2Py was characterized in toluene solution, and upon photoisomerization of NBD-2Py to QC-2Py using a 405 nm LED, the emission measured upon excitation at 373 nm decreases (Figure 3b). This is in line with what has been observed in our previous studies with the fluorescent bis(ethynylphenylene) substituted NBD.[15] Unfortunately, upon extended irradiation at 405 nm the emission did not decrease to zero but we observed a low intensity with a different shape (see SI Figure S8); based on several observations we deduced that a small amount of emissive impurities form upon irradiation. The emission was measured after stepwise irradiations at 405 nm and keeping the sample at 0 °C and under stirring. Interestingly, when the emission was measured with excitation at 310 nm (where the formed QC absorbs), the intensity decreases at a much lower rate than when the emission was measured with excitation at 373 nm, while still

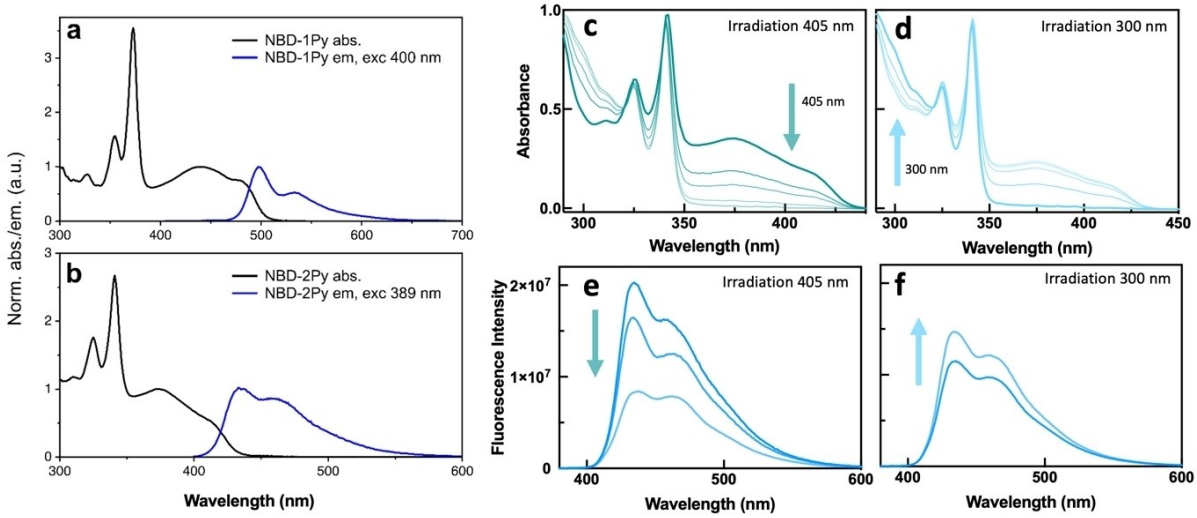

Figure 1. Normalized steady-state absorption and emission of (a) NBD-1Py, and (b) NBD-2Py in toluene. (c) Absorption changes of NBD-2Py isomerising to QC-2Py under 405 nm step-wise irradiations. (d) Absorption changes of QC-2Py isomerising to NBD-2Py under 300 nm step-wise irradiations. (e) Emission changes of NBD-2Py isomerising to QC-2Py under 405 nm step-wise irradiations. (f) Emission changes of Qc-2Py isomerising to NBD-1Py upon 300 nm irradiation.

Table 1. Calculated electronic and photophysical data for the dyes **NBD-1Py** and **NBD-2Py**.[a]

Compound	Absorption Transition	f[b]	Dominant Component (%)[c]	$E_{max\ calc.}$ (eV)[d]	$E_{max\ exp.}$ (eV)[d]	$\Delta E_{HOMO\text{-}LUMO}$ (eV)[e]
NBD-1Py	$S_1 \leftarrow S_0$	0.996	LUMO←HOMO (88)	2.77	2.82	4.84
	$S_2 \leftarrow S_0$	1.085	LUMO←HOMO-1 (50) LUMO+1←HOMO (42)	3.51		
NBD-2Py	$S_1 \leftarrow S_0$	1.216	LUMO←HOMO (92)	3.18	3.32	5.48
	$S_2 \leftarrow S_0$	0.003	LUMO←HOMO-1 (37) LUMO+1←HOMO (22)	3.68		
	Emission					
NBD-1Py	$S_1 \rightarrow S_0$	1.057	LUMO→HOMO (94)	2.10	2.48	
NBD-2Py	$S_1 \rightarrow S_0$	0.994	LUMO→HOMO (95)	2.43	2.86	

[a] Calculated by TD-DFT at level PCM(toluene)/CAM–B3LYP/cc-pVDZ, corresponding to the $S_1 \leftarrow S_0$ and $S_2 \leftarrow S_0$ (absorption) and $S_1 \rightarrow S_0$ transitions (emission). [b] Oscillator strength. [c] Percentage contribution approximated by 2 x $(c_i)^2$ ×100%. [d] Calculated (calc.) and experimental (exp.) energies. [e] Calculated HOMO-LUMO energy band gap.

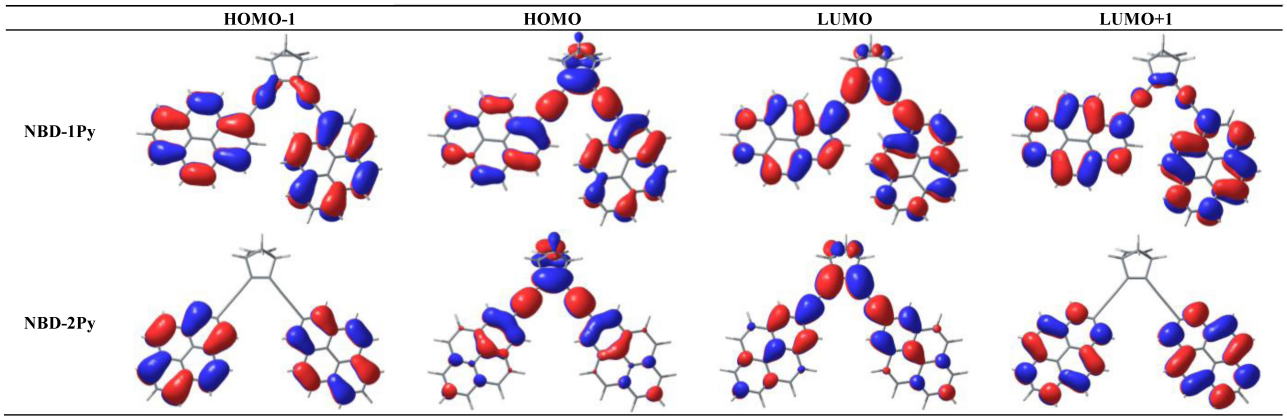

Figure 2. Molecular orbitals of NBD-1Py and NBD-2Py.

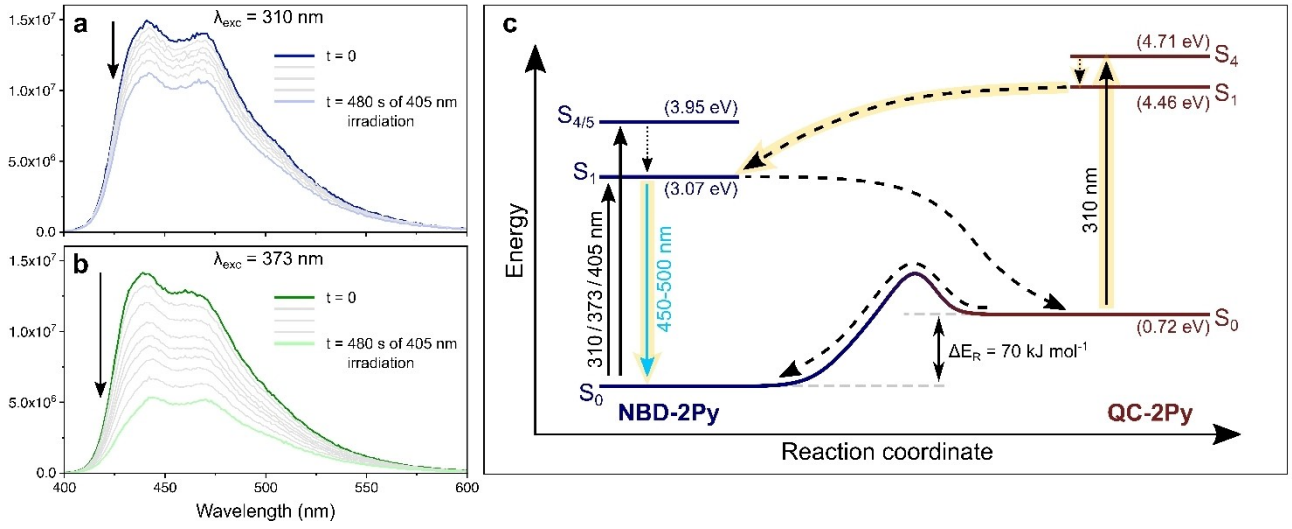

Figure 3. Steady state emission of NBD-2Py measured directly after different times (0-480 s) of exposure to 405 nm continuous-wave irradiation at 0°C. (a) λexc = 310 nm. (b) λexc = 373 nm. (c) Proposed reaction pathways in NBD-2Py. Highlighted in yellow is the suggested reaction pathway of photoinitiated backconversion from QC-2Py to NBD-2Py.

retaining the spectral shape of the NBD fluorescence (Figure 3a). Even after maximised isomerization of NBD to QC and with the solution kept at 0 °C to minimize thermal back isomerization, the emission remains (see SI Figure S8). While QC could theoretically emit given its pyrene moieties, the measured emission upon excitation at 310 nm resembles that of NBD, both in spectral shape and wavelength of emission, contradicting this hypothesis. Therefore, we believe this is indicative of QC back photoconverting to the NBD form on the excited state surface (S1), followed by emission from the first singlet excited state of NBD. The observed photoisomerization induced fluorescence through adiabatic photoisomerization is (to the best of our knowledge) reported here for the first time in these systems; importantly, an adiabatic QC to NBD photoisomerization mechanism would be different than what has been previously reported.[24]

The samples used for the spectroscopy studies had low concentrations which would prevent eventual intermolecular interactions between pyrenes the units. Based on the known literature regarding emissive excimer formations between spatially close pyrene moieties[19,25] we investigated the eventual presence of intramolecular excimers in NBD-2Py/QC-2Py. We did not observe any emission indicative of excimer formation in any of the two isomers, which could be due to unfavourable orientation of the pyrene moieties or other processes preventing it.

The robustness of the NBD-2Py over multiple cycles of photoisomerization and thermal back-conversion was also characterized in solution. The relatively short back-conversion time allowed the utilization of an automated setup connected to a spectrofluorimeter, which controlled sample temperature (80°***C***) and irradiation intervals with a 405 nm LED. We completed 120 cycles (Figure 4), and notably, NBD-2Py exhibited remarkable stability against photodegradation at this excitation wavelength. Consequently, we conducted a longer photo-thermal cycling experiment, subjecting NBD-2Py to 3000 cycles (in SI, section 5). After 3000 cycles (6000 isomerization reactions) more than 33% of the original NBD compound was successfully recovered. The exceptional stability of NBD-2Py makes it an intriguing candidate for applications in optical memory storage, bioimaging,[2c] and other fields.

Crystal Structures Characterization

To gain insights into the exact molecular geometry, crystals of the two norbornadienes have been obtained in the mixture of DCM/Hexane (1:10) and characterised; more crystal data and refinement parameters of NBD-1Py and NBD-2Py are given in Table S1, section 2 in the SI. NBD-1Py crystallized in the monoclinic space group $P2_1/c$ (Z = 4) and its asymmetric unit comprises two molecules of NBD-1Py. There is a disorder between one of the 5 membered rings with a higher occupancy of 0.84. Notably NBD-1Py adopts an unsymmetric conformation, perhaps to optimize molecular packing. This packing is mainly governed by π···π stacking between NBD-1Py pyrene rings with the shortest distance at 3.508 (2) Å as this is the main interaction in the crystal structure. Other weak interactions such as C–H···π are also perceived with the shortest distance at 2.700 (1) Å (Figure 5a,b). The packing diagram shows zigzag layers of the NBD-1Py molecules down the z-axis and Hirshfeld surface analysis,[26] as seen in Figure 5c. The NBD-2Py crystal structure is a solvate containing hexane. The structure was solved in an orthorhombic space group Pnma (Z = 8) with its asymmetric unit showing half a molecule of NBD-2Py and 0.25 hexane but for a better refinement, the hexane was squeezed using solvent mask in Olex 2 software (Figure 5d).[27] The NBD-2Py hexane solvate is mostly governed by a huge number of π···π interactions between NBD-2Py membered rings with the shortest distance measured at 3.377 (2) Å. There are eight C–H···π also perceived with a minimum distance at 2.720 (3) Å. Figure 5e shows that the hexane solvent is located down [100] running through NBD-2Py channels in the structure with a void volume (solvent accessible surface) of 97.3 Å^3 and a unit cell volume percentage of 3.2% at a probe radius of 1.2 Å, calculated using Mercury software. These channels have an approximate diameter of 4.4 Å as measured by CrystalMaker software. Figure 5f shows the Hirshfeld surface analysis for NBD-2Py. Further analysis indicate that the structure of NBD-2Py can be seen as a network[28] of C–H···π and π···π interactions where each pyrene connects to three other pyrenes and then also *via* the norbornadiene bridge to form the four-connected **sra**-net,[29] see Figure 5g. Deposition Numbers 2302599 for NBD-1Py and 2302598 for NBD-2Py contain the supplementary crystallographic data for this paper. These data are provided free of charge by the joint Cambridge Crystallographic Data Centre

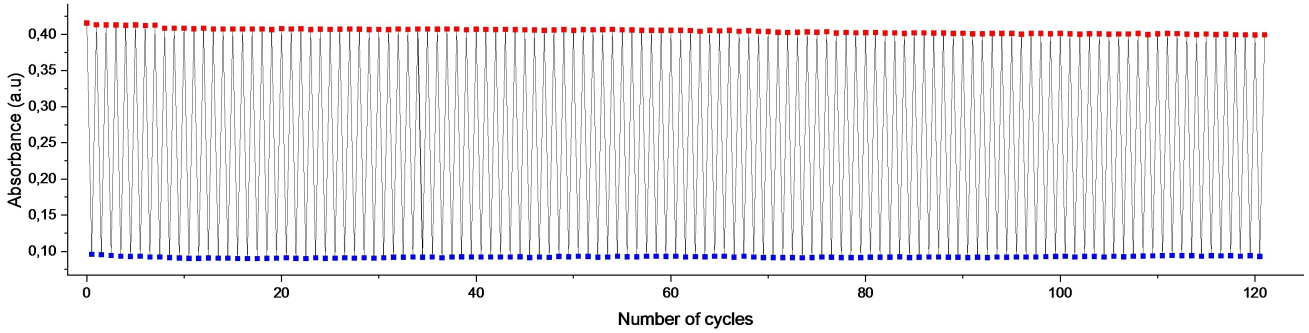

Figure 4. Absorption of NBD-2Py and QC-2Py at 392 nm through 120 cycles of photo and thermal switching.

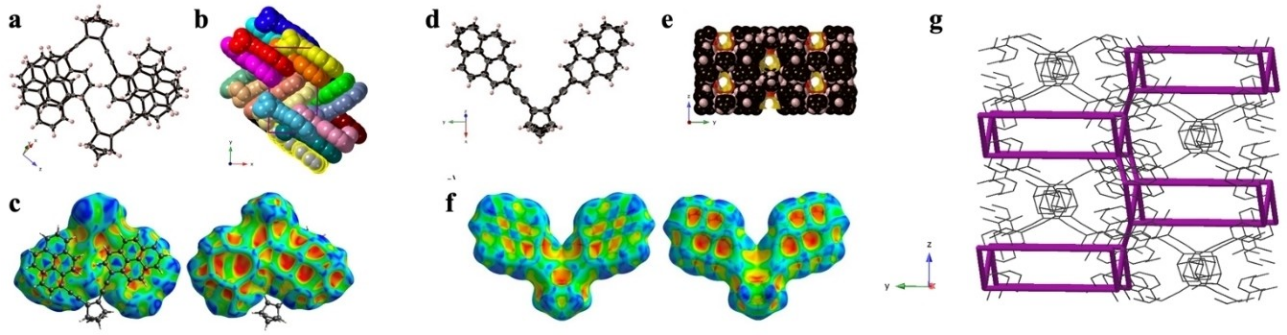

Figure 5. a) Molecular structure of NDB-1Py crystal, with displacement ellipsoids drawn at 50% probability level. b) Packing along z-axis, hydrogen atoms have been omitted and every NDB-1Py molecule coloured individually. c) Hirshfeld surface analysis, showing the shape index mapping. The triangular pattern showing in the left picture is indicative of π···π stacking and the rifts and valleys to the right signals C–H···π interactions. d) The molecular structure of NDB-2Py crystal, with displacement ellipsoids drawn at 50% probability level. e) Packing of NBD-2Py along x-axis using a space filling model (vdW radii), emphasizing the channels in which the hexane molecules are located (these cannot be modelled correctly). f) Hirshfeld surface analysis, showing the shape index mapping. The triangular pattern showing in the left picture is indicative of π···π stacking and the rifts and valleys to the right signals C–H···π interactions. g) Network topology analysis of NBD-2Py based on C–H···π and π···π interactions has each pyrene connecting to three other pyrenes and then also via the norbornadiene bridge to form the four-connected sra-net shown in burgundy. C–C bonds in black and hydrogens have been omitted.

and Fachinformationszentrum Karlsruhe at http://www.ccdc.cam.ac.uk/structures.

NBD-Py as Photoswitchable Probes for Fluorescent Imaging of Alzheimer Pathology In Situ

Confocal and Hyperspectral Imaging

We evaluated pyrene substituted norbornadienes (NBD–Py) as fluorescent probes targeting Aβ pathology in mouse model tissues.

Moreover, we characterized the switching behaviour of NBD-2Py *in situ*. We used frozen brain sections (12 μm) from 21 month-old female transgenic tgAPPSwe AD mice models. This transgenic model have the human APP gene bearing the Swedish mutation, therefore expressing human Aβ peptide. At 21 months, tgAPPSwe mice are characterized by a high plaque load of large cored plaques in both the prefrontal cortex and hippocampus.[30] The tissue sections were mounted on microscope slides and after fixation and washing they were stained with an ethanol solution of NBD-1Py or NBD-2Py for 2 h (detailed method in SI) yielding clearly stained amiloyd plaques (Figure 6a and SI). To validate the probes target, co-staining of NBD-1Py and NBD-2Py with 6E10 anti beta amyloid antibody was also performed. NBD-2Py staining (Figure 6c in green) and NBD-1Py (SI) both demonstrate excellent co-localisation with 6E10 antibody (in red), confirming what is clearly visually assessed: NBD-1Py and NBD-2Py effectively target and stain Aβ plaques in TgSwe mouse models tissue. Hyperspectral confocal imaging using a Carl Zeiss LSM 880 Airyscan was done to assess the spectral properties of NBD-2Py *in situ* (Figure 6a). A 405 nm LED is used to irradiate the sample, and the emission is measured between 420 and 600 nm at 9 nm intervals. The signal was measured in Fiji and averaged over the whole plaques area. It shows how the fluorescence emission profile of NBD-2Py is not significantly affected by the binding, as seen in Figure 6b. Given that the pyrene moieties are larger than the long conjugated "arms" of the bis(ethynylphenylene) substituted NBD we previously investigated,[15] we think it is unlikely that they can bind to the same narrow pocket. For this reason, we chose to investigate further the binding modes with Aβ plaques by performing molecular docking simulations of the norbornadienes with Aβ aggregates.

Molecular Docking Studies

Molecular docking simulations were performed to evaluate the interactions between the NBD–Py and the Aβ plaques. We have chosen solid-state NMR structures (PDB ID: 2LMP) as a model for the Aβ1-40 plaques and (PDB ID: 2MXU) for Aβ1-42 plaques. The obtained binding affinities were slightly higher for Aβ1-40 (2LMP) amyloid, with a docking score of −14.1 kcal/mol for both NBD–Py. Comparatively, for Aβ1-42 (2MXU) structure the docking scores were −12.7 and −12.1 kcal/mol for NBD-1Py and NBD-2Py respectively. Regarding the Aβ1-40 amyloid model, NBD-2Py interacts with the 2LMP structure in a different domain than NBD-1Py (see SI section 6), placing one of its pyrene-arms inside a tunnel (Figure 6e and 6f) displaying π-σ interactions with Ala and Ile residues (Figure 6f). The internal cavity of this tunnel exhibits a hydrophobic environment mainly composed of the following nonpolar amino acids: Ala, Leu, Ile and Phe (more detailed images and information of the binding sites are in SI Section 6). The other pyrene arm engages in π···π stacking interactions with the Phe residues at the beginning of the tunnel (Figure 6f). The docking simulations with the Aβ1-42 amyloid model yield similar results for both compounds. Both structures are located on a hydrophobic groove of the 2MXU model (Figure 6g, h for NBD-2Py, Figures for NBD-1Py are in SI Section 6).

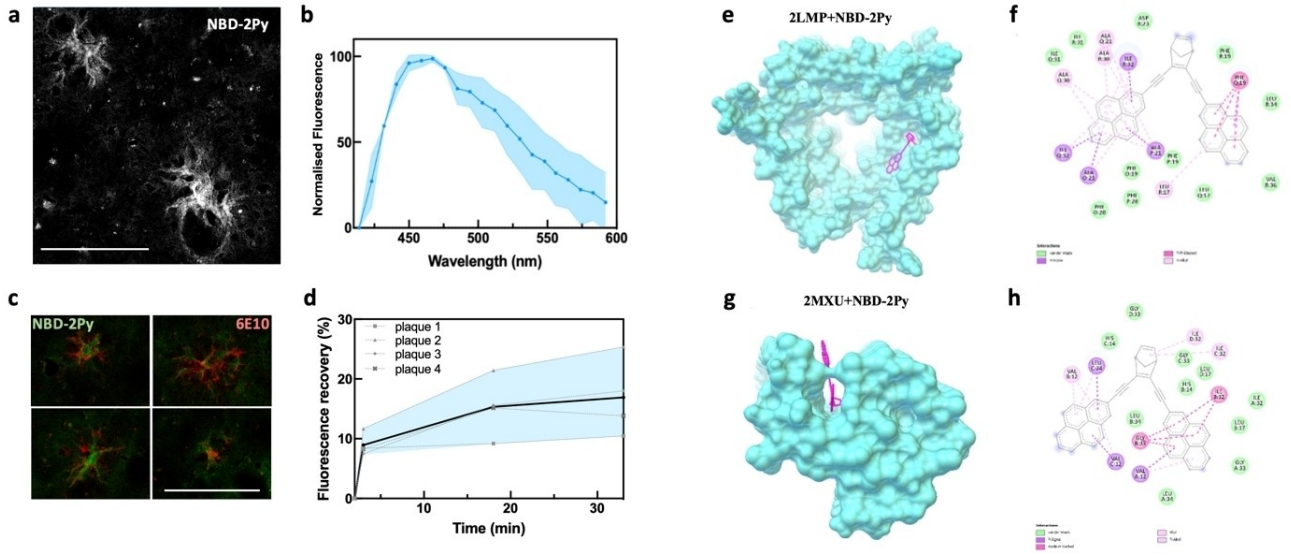

Figure 6. a) Confocal image of Aβ plaques in the cortex of brain sections of a TgSwe mouse model (21 months, female) obtained with NBD-2Py as a fluorescent stain. White bar = 100 μm. In situ measured emission spectra of NBD-2Py (b) when staining the plaques. Measures are an average of the 2 plaques areas, and range is shown as a blue band. c) Confocal images of Aβ plaques in the cortex of brain sections of a TgSwe mouse model (21 months, female). Green is NBD-2Py, red is 6E10 anti amyloid-β antibody; White bar = 100 μm. d) Recovery of NBD-2Py fluorescence signal over time after irradiation of the plaque's areas; 4 plaques are measured, and average and range of recovery are shown as blue lines and area respectively. 17% of recovery in average is observed after around 30 minutes. e), f) Binding modes of NBD-2Py with the Aβ1-40 (PDB ID: 2LMP) amyloid plaque. e) 3D image of the NBD-2Py-2LMP complex (surface of the receptor in light-blue and ligand in magenta). f) 2D interaction diagram of the interactions of NBD-2Py with 2LMP. g) h) Binding modes for NBD-2Py with the Aβ1-42 (PDB ID: 2MXU) amyloid plaque. g) 3D image of NBD-2Py-2MXU ligand-receptor (surface of the receptor in light-blue and ligand in magenta). h) 2D interaction diagram of the interactions of NBD-2Py with 2MXU.

This groove is mainly composed of Gly, Ala, Leu and Ile amino acid residues, with π-σ and van der Waals interactions occurring between the NBD–Py compounds (more details in SI section 6). Overall, NBD–Py exhibits improved calculated binding to amyloid models compared to the previously investigated bis(ethynylphenylene) substituted NBD, which is mainly achieved thanks to insertion into hydrophobic sites in the plaques where the pyrene moieties are surrounded by non-polar amino acids.

Fluorescence Photo-Switching In Situ

We investigated the photo-switching properties of NBD-2Py *in situ*. NBD-2Py stained AD mouse brain sections were irradiated with the confocal microscope light source (405 nm LED). Using the same Zeiss LSM 880 Airyscan microscope, the experiment was set to provide intense light irradiation (405 nm LED at 10% of intensity), followed by image acquisition every 5 seconds (405 nm LED at 1% intensity) for a total of 2 minutes. To capture the whole plaques which are three-dimensional objects, z-scan images were acquired each time, and the maximum intensity projection (obtained using Zeiss in-built processing tool) was used for signal intensity analysis. Subsequently, the intense irradiation was stopped, the imaged area was extended by zooming out (to monitor not irradiated plaques as well and to assess photobleaching), and images were acquired at regular intervals of 15 minutes. The signal from the irradiated plaques increased over time after the intense irradiation was stopped (despite slight photobleaching effects due to image acquisition), indicating back-conversion of QC-2Py to the fluorescent NBD-2Py *in situ*. The fluorescence signal was analysed over 4 different plaques, with different sizes and morphology; the whole plaque's area was considered, with ROI selected using in-built Fiji thresholds (Moments), and the whole spectra extracted for these plaques over the experiments time. The peaks areas were plotted over time, and it can be seen in Figure 6d how they increase significantly: after only around 30 minutes we observe an average of 17% signal recovery, with a maximum of 25% recovery in plaque 2. This is a significant improvement compared to the previously reported bis(ethynylphenylene) substituted NBD (where 24% of signal recovery was achieved after 240 minutes), both because of increased signal recovery and faster recovery times. Nonetheless, almost quantitative recovery with a shorter time span (e.g. ms) is necessary for applications within super-resolution imaging.[3a,21]

Conclusions

We present the synthesis and characterization of two novel pyrene substituted fluorescent NBD (NBD-1Py and NBD-2Py). Chemical, spectroscopic, and crystal structure characterisation of the two molecular systems are presented and discussed, with support of DFT calculations. It is observed that their spectral properties are significantly different, with NBD-1Py absorption and emission bands red-shifted compared to NBD-2Py. This is rationalised based on their calculated molecular orbitals which show extended conjugation over the whole molecule in NBD-

1Py. Effects of the photoisomerization on the emission of NBD-2Py solutions are investigated; photoisomerization of NBD-2Py to QC-2Py induces a decrease in the fluorescence signal. Surprisingly, when exciting QC-2Py at 310 nm we observe higher luminescence than when exciting only NBD at 373 nm, and we hypothesize how this is due to light-induced back isomerization to the excited NBD-2Py which is then the emitting specie. These observations offer an insight into the QC to NBD photoisomerization mechanism which is for the first time observed following an adiabatic pathway followed by emission. Furthermore, NBD-1Py and NBD-2Py efficiently stain Aβ plaques in TgSwe mouse model tissues; their spectroscopic and switching properties are characterised *in situ* and their binding mode is described through docking simulations. Notably, they offer several improvements compared to the previously considered bis(ethynylphenylene) substituted NBD, including improved calculated binding to Aβ aggregates, shorter QC to NBD back-conversion time, higher switching efficiency, and enhanced cyclability. While these are very promising advances, some challenges are still to be addressed. The main future goals will be for example to improve the solubility in aqueous systems and faster QC to NBD isomerization in tissue, which when achieved would unlock applications for advanced imaging of Alzheimer pathology.

Author Contributions

SG, AD and KMP conceptualized the project. SG and KMP conceptualized the molecules, SG did the synthesis and analytical characterization of the compounds. SG and AD performed the spectroscopic characterisations together with AO, FE, ASA, ZW, MS, and WL. EH, RS, AO, BA, FN contributed to interpret the spectroscopic results. AD and JH provided the bio-imaging study. AEH–B KVM and FN provided DFT calculations, FN and EP–I provided the docking study, LÖ and FMAN provided the X-ray structures. SG, AD, FN and KM–P wrote and revised the manuscript with contributions from all the co-authors.

Acknowledgements

Microscopy images were acquired at the Centre for Cellular Imaging (CCI), Core Facilities, the Sahlgrenska Academy, University of Gothenburg. Chalmers Material Analysis Laboratory, CMAL is acknowledged for crystals characterizations, and we thank the Olle Engkvist Foundation for funding the single crystal diffractometer. We are grateful for the

access to the Supercomputing and Bioinformatics Center (University of Málaga) and the provided technical support.

The following agencies are acknowledged for financing the presented work: Spanish Ministerio de Ciencia e Innovación (grant PID2022-136705NB–I00; Proyectos de I + D + I Programación Conjunta Internacional, Euro-NanoMed 2019 (PCI2019-111825-2); International Postdoc Grant of the Swedish Research Council VR (#2021-00478); Swedish Energy Agency; the Göran Gustafsson Foundation; the Swedish Research Council; the Chalmers Foundation; Swedish Research Council Formas; the European Research Council (ERC) under grant agreement CoG, PHOTHERM – 101002131; the Catalan Institute of Advanced Studies (ICREA); and the European Union's Horizon2020 Framework Programme under grant agreement no. 951801.

Conflict of Interests

The authors declare no conflict of interest.

Data Availability Statement

Most relevant data are available in the SI, but further information and raw data can be requested to the authors.

Keywords: Norbornadienes · photochromism · photoswitches · imaging · Alzheimer

[1] G. Smith, *J. Mater. Sci.* **1967**, *2*, 139–152.
[2] a) W. Szymanski, J. M. Beierle, H. A. Kistemaker, W. A. Velema, B. L. Feringa, *Chem. Rev.* **2013**, *113*, 6114–6178; b) A.-A. Nahain, J.-E. Lee, J. H. Jeong, S. Y. Park, *Biomacromolecules* **2013**, *14*, 4082–4090; c) Z. Tian, A. D. Li, *Acc. Chem. Res.* **2013**, *46*, 269–279.
[3] a) M. Minoshima, K. Kikuchi, *JBIC Journal of Biological Inorganic Chemistry* **2017**, *22*, 639–652; b) E. A. Halabi, D. Pinotsi, P. Rivera-Fuentes, *Nat. Commun.* **2019**, *10*, 1232; c) O. Nevskyi, D. Sysoiev, J. Dreier, S. C. Stein, A. Oppermann, F. Lemken, T. Janke, J. Enderlein, I. Testa, T. Huhn, *Small* **2018**, *14*, 1703333.
[4] a) W. A. Velema, W. Szymanski, B. L. Feringa, *J. Am. Chem. Soc.* **2014**, *136*, 2178–2191; b) J. Broichhagen, J. A. Frank, D. Trauner, *Acc. Chem. Res.* **2015**, *48*, 1947–1960.
[5] a) K. Mutoh, N. Miyashita, K. Arai, J. Abe, *J. Am. Chem. Soc.* **2019**, *141*, 5650–5654; b) R. Kashihara, M. Morimoto, S. Ito, H. Miyasaka, M. Irie, *J. Am. Chem. Soc.* **2017**, *139*, 16498–16501; c) S. Helmy, F. A. Leibfarth, S. Oh, J. E. Poelma, C. J. Hawker, J. Read de Alaniz, *J. Am. Chem. Soc.* **2014**, *136*, 8169–8172.
[6] M. Olesińska-Mönch, C. Deo, *Chem. Commun.* **2023**, *59*, 660–669.
[7] R. Bresolí-Obach, W. A. Massad, A. Abudulimu, L. Lüer, C. Flors, J. G. Luis, L. I. Rosquete, T. A. Grillo, O. Anamimoghadam, G. Bucher, *Dyes Pigm.* **2021**, *186*, 109060.
[8] G. Naren, W. Larsson, C. Benitez-Martin, S. Li, E. Pérez-Inestrosa, B. Albinsson, J. Andréasson, *Chem. Sci.* **2021**, *12*, 7073–7078.
[9] G. Lv, B. Cui, H. Lan, Y. Wen, A. Sun, T. Yi, *Chem. Commun.* **2015**, *51*, 125–128.
[10] D. Kim, A. Aktalay, N. Jensen, K. Uno, M. L. Bossi, V. N. Belov, S. W. Hell, *J. Am. Chem. Soc.* **2022**, *144*, 14235–14247.
[11] a) Z. Wang, A. Roffey, R. Losantos, A. Lennartson, M. Jevric, A. U. Petersen, M. Quant, A. Dreos, X. Wen, D. Sampedro, *Energy Environ. Sci.* **2019**, *12*, 187–193; b) M. Mansø, A. U. Petersen, Z. Wang, P. Erhart, M. B. Nielsen, K. Moth-Poulsen, *Nat. Commun.* **2018**, *9*, 1945; c) Z. Wang, P. Erhart, T. Li, Z.-Y. Zhang, D. Sampedro, Z. Hu, H. A. Wegner, O. Brummel, J. Libuda, M. B. Nielsen, *Joule* **2021**, *5*, 3116–3136; d) Z. Wang, H. Hölzel, K. Moth-Poulsen, *Chem. Soc. Rev.* **2022**; e) F.-Y. Meng, I.-H. Chen, J.-Y. Shen, K.-H. Chang, T.-C. Chou, Y.-A. Chen, Y.-T. Chen, C.-L. Chen, P.-T. Chou, *Nat. Commun.* **2022**, *13*, 797.
[12] a) B. E. Tebikachew, H. B. Li, A. Pirrotta, K. Börjesson, G. C. Solomon, J. Hihath, K. Moth-Poulsen, *J. Phys. Chem. C* **2017**, *121*, 7094–7100; b) H. B. Li, B. E. Tebikachew, C. Wiberg, K. Moth-Poulsen, J. Hihath, *Angew. Chem.* **2020**, *132*, 11738–11743.
[13] A. Dreos, J. Ge, F. Najera, B. E. Tebikachew, E. Perez-Inestrosa, K. Moth-Poulsen, K. Blennow, H. Zetterberg, J. r. Hanrieder, *ACS Sens.* **2023**, *8*, 1500–1509.
[14] V. A. Bren, A. D. Dubonosov, V. I. Minkin, V. A. Chernoivanov, *Russ. Chem. Rev.* **1991**, *60*, 451–469.

[15] B. E. Tebikachew, F. Edhborg, N. Kann, B. Albinsson, K. Moth-Poulsen, *Phys. Chem. Chem. Phys.* **2018**, *20*, 23195–23201.
[16] J. Hardy, D. Allsop, *Trends Pharmacol. Sci.* **1991**, *12*, 383–388.
[17] M. Fändrich, S. Nyström, K. P. R. Nilsson, A. Böckmann, H. LeVine III, P. Hammarström, *J. Intern. Med.* **2018**, *283*, 218–237.
[18] Y. W. Jun, S. W. Cho, J. Jung, Y. Huh, Y. Kim, D. Kim, K. H. Ahn, *ACS Cent. Sci.* **2019**, *5*, 209–217.
[19] G. Bains, A. B. Patel, V. Narayanaswami, *Molecules* **2011**, *16*, 7909–7935.
[20] a) J. Zhang, A. Sandberg, X. Wu, S. Nyström, M. Lindgren, P. Konradsson, P. Hammarström, *ACS Omega* **2017**, *2*, 4693–4704; b) J. Zhang, J. Wang, A. Sandberg, X. Wu, S. Nyström, H. LeVine III, P. Konradsson, P. Hammarström, B. Durbeej, M. Lindgren, *ChemPhysChem* **2018**, *19*, 3001–3009.
[21] J. Valli, J. Sanderson, *Current Protocols* **2021**, *1*, e224.
[22] A. Lennartson, M. Quant, K. Moth-Poulsen, *Synlett* **2015**, *26*, 1501–1504.
[23] A. G. Crawford, A. D. Dwyer, Z. Liu, A. Steffen, A. Beeby, L.-O. Palsson, D. J. Tozer, T. B. Marder, *J. Am. Chem. Soc.* **2011**, *133*, 13349–13362.
[24] W. Alex, P. Lorenz, C. Henkel, T. Clark, A. Hirsch, D. M. Guldi, *J. Am. Chem. Soc.* **2021**, *144*, 153–162.
[25] M. Barale, M. Escadeillas, G. Taupier, Y. Molard, C. Orione, E. Caytan, R. Métivier, J. Boixel, *J. Phys. Chem. Lett.* **2022**, *13*, 10936–10942.
[26] M. A. Spackman, D. Jayatilaka, *CrystEngComm* **2009**, *11*, 19–32.
[27] O. V. Dolomanov, L. J. Bourhis, R. J. Gildea, J. A. K. Howard, H. Puschmann, *J. Appl. Crystallogr.* **2009**, *42*, 339–341.
[28] a) L. Öhrström, *Chem. Eur. J.* **2016**, *22*, 13758–13763; b) F. Hoffmann, M. Fröba, in *The Chemistry of Metal-Organic Frameworks: Synthesis, Characterization, and Applications*, (Ed.: S. Kaskel), John Wiley & Sons, **2016**; c) O. Delgado-Friedrichs, S. T. Hyde, M. O'Keeffe, O. M. Yaghi, *Struct. Chem.* **2017**, *28*, 39–44.
[29] a) M. O'Keeffe, M. A. Peskov, S. Ramsden, O. M. Yaghi, *Acc. Chem. Res.* **2008**, *41*, 1782–1789; b) M. O'Keeffe, O. Delgado-Friedrichs, (Ed.: O. K. Reticular Structure Chemistry Resource, M.; Yaghi, O. M.; Ramsden, S.), **2019**.
[30] a) O. Philipson, P. Hammarström, K. P. R. Nilsson, E. Portelius, T. Olofsson, M. Ingelsson, B. T. Hyman, K. Blennow, L. Lannfelt, H. Kalimo, *Neurobiol. Aging* **2009**, *30*, 1393–1405; b) M. Pagnon de la Vega, V. Giedraitis, W. Michno, L. Kilander, G. Güner, M. Zielinski, M. Löwenmark, R. Brundin, T. Danfors, L. Söderberg, *Sci. Transl. Med.* **2021**, *13*, eabc6184.

Manuscript received: January 26, 2024
Accepted manuscript online: April 17, 2024
Version of record online: ■■, ■■

RESEARCH ARTICLE

In this study we synthesize and characterise two novel fluorescent norbornadiene derivatives bearing pyrene moieties. In depth spectral and physico-chemical characterisation is presented; moreover, their application as dyes for imaging of amyloid beta aggregates in Alzheimer's mice models is investigated, with implications for bioimaging and protein aggregate studies.

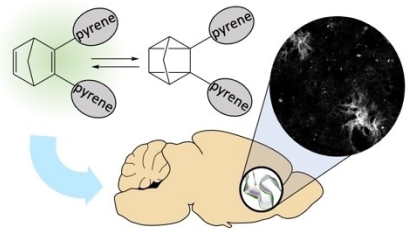

S. Ghasemi, M. Shamsabadi, A. Olesund, F. Najera, A. Erbs Hillers-Bendtsen, F. Edhborg, A. S. Aslam, W. Larsson, Z. Wang, F. M. Amombo Noa, R. J. Salthouse, L. Öhrström, H. Hölzel, E. Perez-Inestrosa, K. V. Mikkelsen, J. Hanrieder, B. Albinsson, A. Dreos, K. Moth-Poulsen**

1 – 10

Pyrene Functionalized Norbornadiene-Quadricyclane Fluorescent Photoswitches: Characterization of their Spectral Properties and Application in Imaging of Amyloid Beta Plaques